American Mineralogist, Volume 76, pages 1628–1645, 1991

Volatiles and lithophile elements in Taylor Creek Rhyolite: Constraints from glass inclusion analysis

JAMES D. WEBSTER*
Grant Institute of Geology, King's Buildings, West Mains Road, University of Edinburgh, Edinburgh EH93JW, Scotland
WENDELL A. DUFFIELD
U.S. Geological Survey, 2255 North Gemini Drive, Flagstaff, Arizona 86001, U.S.A.

ABSTRACT

Glass-bearing inclusions in quartz phenocrysts from four eruptive units of the F-rich, Sn-mineralized Taylor Creek Rhyolite, New Mexico, have been analyzed by electron microprobe. Inclusions from two units contain F-rich glass and the daughter minerals fluor-biotite (>4 wt% F), fluorite, and fluor-muscovite (>6 wt% F); these fractions of magma contained extreme concentrations of F. Glass-rich inclusions from the other two units have also been analyzed by ion microprobe for H, Li, Rb, Cs, Ce, Be, Sr, Y, Nb, U, Th, Mo, W, Sn, and B. Close similarities in major-element composition between these glass-rich inclusions and host whole rocks indicate that the inclusions are samples of melt from which the phenocrysts grew. F contents of these glass inclusions are variable and low relative to inclusions containing micas and fluorite.

Concentrations of Al_2O_3, Na_2O, K_2O, H_2O, FeO, and CaO in glass-rich inclusions vary and correlate inversely with SiO_2. This is interpreted to indicate that up to 15 wt% SiO_2 crystallized within inclusions after trapping of melt, although secondarily precipitated quartz is not optically visible within inclusions. This postentrapment process does not measurably change trace-element concentrations in trapped glass relative to analytical uncertainty.

Concentrations of minor and trace elements in glass inclusions vary by factors of 2 to >10. These variations are significantly greater than those shown by whole rocks, indicate that melt was strongly heterogeneous for some trace elements, and express melt evolution as phenocrysts grew. Mean concentrations of Rb, Cs, and Cl (± U) in glass inclusions exceed those in glassy whole rocks; the concentrations of these and other relatively mobile elements (H_2O and Li) in vitrophyres do not represent the composition of parent melt. Relatively low H_2O and high Cl concentrations in melt imply that these fractions of melt were H_2O undersaturated prior to trapping of inclusions. Preeruptive H_2O content of melt, from which quartz phenocrysts grew, was ≤2.7 wt%. Preeruptive abundances of other mobile constituents in this melt were 0.25 wt% F, 0.26 wt% Cl, 45 ppm B, 11 ppm U, 16 ppm Cs, and 15 ppm Sn. Mobile constituents were variably removed from Taylor Creek Rhyolite magma during or after eruption but after melt inclusions were entrapped in quartz. Mean concentrations of immobile trace elements in glass inclusions are equivalent to those in whole rocks.

INTRODUCTION

Highly evolved silicic magmas, including tin and topaz rhyolites, are variably enriched in the volatiles, H_2O, CO_2, F, Cl, and B and in the lithophile elements Sn, W, Mo, U, Th, Ta, Nb, Be, Rb, Cs, Li, and others (Christiansen et al., 1986) and may be genetically associated with lithophile mineralization (Pan, 1974; Burt and Sheridan, 1981; Burt et al., 1982; Huspeni et al., 1984; Duffield et al., 1990). Investigations of the petrogenesis and differentiation of chemically evolved silicic magmas and of associated mineralization should make use of accurate concentrations of all magmatic components of interest. Relatively mobile constituents including H_2O, CO_2, F, Cl, B, S, Sn, and alkali metals, however, may be lost from melt or glass during plutonic emplacement and crystallization and also during and after volcanic eruption. As a result, it is difficult to model these processes accurately in highly evolved, volatile-rich silicic magmas. Concentrations of mobile constituents in felsites and vitrophyres are generally not representative of melt, although glassy volcanic rocks typically provide a more representative sample of melt than crystalline rocks (Noble et al., 1967; Rosholt et al., 1971; Zielinski et al., 1977).

Glass inclusions in volcanic phenocrysts may be rep-

* Present address: Department of Mineral Sciences, American Museum of Natural History, Central Park West at 79th Street, New York, New York 10024-5192, U.S.A.

0003–004X/91/0910–1628$02.00

resentative of the melt from which the phenocrysts grew (Roedder and Weiblen, 1970; Naumov et al., 1971; Anderson, 1973; Beddoe-Stephens et al., 1983; Clocchiatti and Massare, 1985; and many others) and, therefore, are a preferred type of sample for studying volatile-enriched igneous systems. Advances in microanalysis now permit the accurate determination of concentrations of volatiles and trace elements at the parts per million level in samples that are only a few tens of micrometers wide (Anderson et al., 1989; Dunbar et al., 1989; Hervig et al., 1989; Hervig and Dunbar, 1989). H_2O, CO_2, and CO in glass have been determined by mass spectrometry (Sommer, 1977; Chaigneau et al., 1980), and recently Anderson et al. (1989) determined H_2O and CO_2 in glass inclusions by infrared spectroscopy. Other studies have determined H_2O indirectly by measuring H^+ in glass inclusions with secondary-ion mass spectrometry (SIMS) (Delaney and Karsten, 1981; Kovalenko et al., 1988; Hervig et al., 1989; Dunbar et al., 1989; Hervig and Dunbar, 1989; Webster, 1989). Many of these studies (for example, Anderson et al., 1989; Dunbar et al., 1989; Hervig et al., 1989; Hervig and Dunbar, 1989) have concluded that some glass inclusions in phenocrysts are chemically representative of the melt from which the crystals grew.

We have analyzed glass inclusions in quartz phenocrysts of the Taylor Creek Rhyolite, New Mexico, that represent trapped and quenched melt to determine the preeruptive abundances of melt constituents in a F-rich magma that is genetically associated with Sn mineralization. Our objectives are (1) to assess the technique of analyzing glass inclusions for determining magmatic abundances of relatively mobile constituents, (2) to understand better the petrogenesis and evolution of volatile-enriched, high-silica rhyolite lavas through comparison of the compositions of whole-rock samples with those of glass inclusions in phenocrysts, and (3) to help constrain preeruptive volatile and ore element abundances in a magmatic system associated with cassiterite deposits (Duffield et al., 1990). We report ion microprobe and electron microprobe analyses of major elements, the volatiles H_2O, F, Cl, and B, and 13 other lithophile trace elements including Mo, W, and Sn. Chemical evidence indicates that disequilibrium growth processes and post trapping crystallization of quartz have variably modified compositions of inclusions, and we present a general method for evaluating the extent of these secondary changes in composition.

Taylor Creek Rhyolite

The Taylor Creek Rhyolite comprises a group of mid-Tertiary lava domes and flows that crop out in the east-central part of the Mogollon-Datil volcanic field of New Mexico (Fries and Butler, 1943; Elston, 1968; Lufkin, 1976; Elston, 1976; Correa, 1981) (Fig. 1). Recent mapping (Duffield et al., 1987) has identified at least 20 vents for these lavas (Fig. 2) that are interpreted to have leaked from a single chamber underlying the area (Duffield and

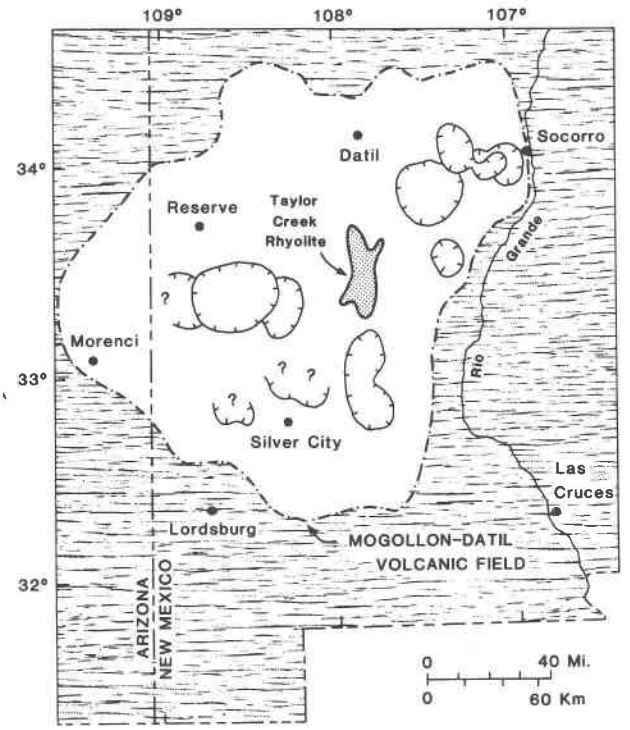

Fig. 1. Map of the Mogollon-Datil volcanic field, New Mexico (Duffield and du Bray 1990); the Taylor Creek Rhyolite is located in the east-central part of the field. Hachured lines signify calderas.

du Bray, 1990); the vents are distributed within a north-elongated rectangular area of several hundred square kilometers. Each vent appears to have been active only once; eruptive activity began with a pyroclastic phase that was followed by the growth of a lava dome or flow. Field evidence suggests that the entire period during which the lava field formed was geologically short, and $^{40}Ar/^{39}Ar$ ages, with a mean about 28 Ma (Duffield and Dalrymple, 1990), indicate that the duration probably was less than 100 000 yr. Conservative reconstruction suggests that domes and flows individually range in volume from less than 1 to about 10 km^3 and cumulatively amount to about 55 km^3. The genetically related pyroclastic deposits likely account for a volume comparable to that of the domes and flows. Cooling histories of individual units are poorly constrained because substantial erosion has occurred at Taylor Creek.

The Taylor Creek Rhyolite is flow foliated and moderately porphyritic. Phenocryst content ranges from about 15 to 35%, and phenocryst size ranges from about 0.5 to 7 mm. The principal minerals are quartz and sanidine in equal to subequal amounts. Plagioclase and altered mafic phenocrysts are ubiquitous at $\leq$1.5% each (Duffield and Dalrymple, 1990). With rare exception, Taylor Creek Rhyolite groundmass is devitrified. About six vitrophyre localities are known, mostly in pyroclastic phases of the rhyolite, and these presumably represent rocks that cooled

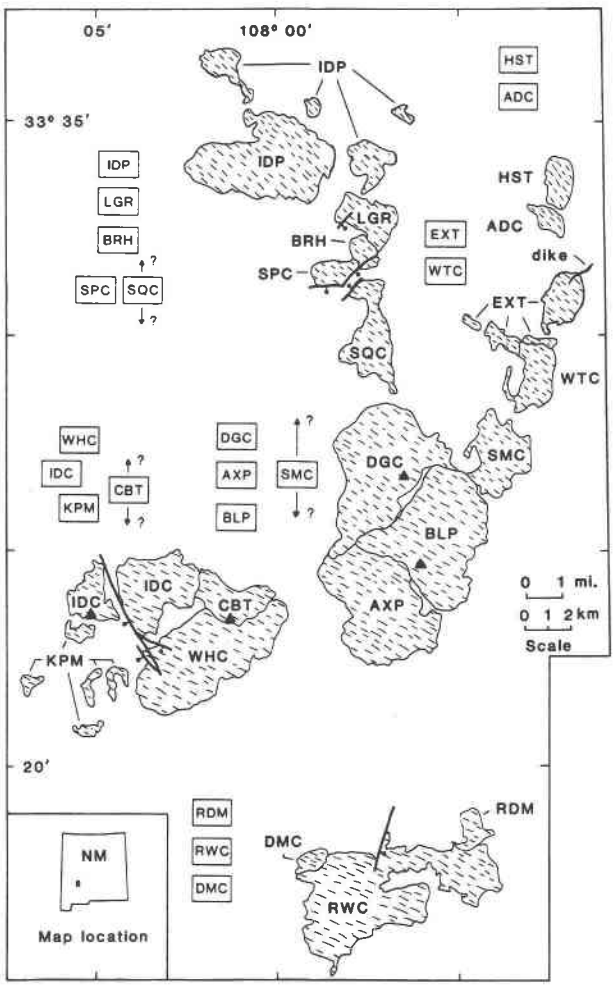

Fig. 2. Geologic map of the Taylor Creek Rhyolite after Duffield et al. (1987); each map unit represents an eruptive unit. Sample localities are shown by solid triangles. Glass inclusions in quartz phenocrysts have been analyzed from rhyolite flows: *IDC* (contains <1 vol% crystals), BLP (crystal rich), DGC (crystal rich), and *CBT* (contains no crystals).

quickly enough to preclude the devitrification that affected the majority of Taylor Creek Rhyolite lavas.

The domes and flows at Taylor Creek comprise a suite of high-silica, metaluminous to weakly peraluminous rhyolites (Duffield and Dalrymple, 1990). Vitrophyres contain considerable H_2O (loss on ignition at 900 °C ranges from about 2 to 3.4 wt%) that is interpreted to result from posteruption, low-temperature hydration. However, this hydration has little or no apparent effect on rock chemistry, except for Li, which is depleted in most vitrophyres relative to felsites (W. A. Duffield, unpublished data). Whole-rock major-element composition varies little (Table 1); mean SiO_2 is about 77.8 ± 0.5 wt% (anhydrous basis). The major-element compositions of the two feldspar-phenocryst species are nearly invariant.

Apparent crystallization temperatures of phenocrysts are somewhat variable, and pressures of crystallization

Table 1. Mean (of 27 analyses) whole-rock and normative compositions of Taylor Creek Rhyolite

Whole-rock major element composition*	Mean	sd**
SiO_2	77.83	0.49
TiO_2	0.13	0.02
Al_2O_3	12.16	0.31
FeO†	1.01	0.08
MnO	0.05	0.01
MgO	<0.12	
CaO	0.30	0.11
Na_2O	3.36	0.36
K_2O	4.92	0.11
P_2O_5	<0.02	
Total‡	99.76	

Normative composition	
Q	38.68
C	0.80
Or	29.05
Ab	28.46
An	1.37
Hy	0.30
Il	0.11
Hm	1.11
Ru	0.08
Ap	0.04
Total	100.00

Note: Data set includes at least one sample from each of the 20 map units of Duffield et al. (1987). Whole-rock analyses are on a volatile-free basis.

* Major element concentrations in weight percent.

** Standard deviation (1σ).

† Total Fe as FeO.

‡ Total does not include wt% MgO or P_2O_5.

are not adequately constrained. Two-feldspar geothermometry suggests that sanidine and oligoclase grew from Taylor Creek Rhyolite magma at temperatures within the range of about 775 °C (Fuhrman and Lindsley, 1988, geothermometer) to 840 °C (Price, 1985, geothermometer). Fe-Ti-oxide geothermometry suggests an equilibration temperature of about 800 °C (Duffield and du Bray, 1990). The timing of quartz crystallization and of melt entrapment, relative to that of feldspar and oxides, is unknown. Preliminary interpretation of the compositions of amphibole phenocrysts in vitrophyre (Wendell A. Duffield, unpublished data), vis-a-vis the geobarometer of Johnson and Rutherford (1989), suggests that the amphiboles crystallized in the 1.5–2 kbar range.

The Taylor Creek Rhyolite contains cassiterite-bearing veins and cassiterite crystals in miarolitic cavities in some localities. Collectively, chemical, physical, and geologic evidence indicates that the lavas were the source of Sn for the mineralization. In this regard, it is important to determine accurate magmatic Sn abundances. Automineralization occurred in the outer and cooler parts of domes or flows; Sn was apparently released during high-temperature devitrification (Correa, 1981; Burt and Sheridan, 1981; Duffield et al., 1990).

Some of the domes and flows also contain topaz crystals of vapor-phase origin in miarolitic cavities, and accordingly Taylor Creek Rhyolite has been classified as topaz rhyolite (for example, Christiansen et al., 1986).

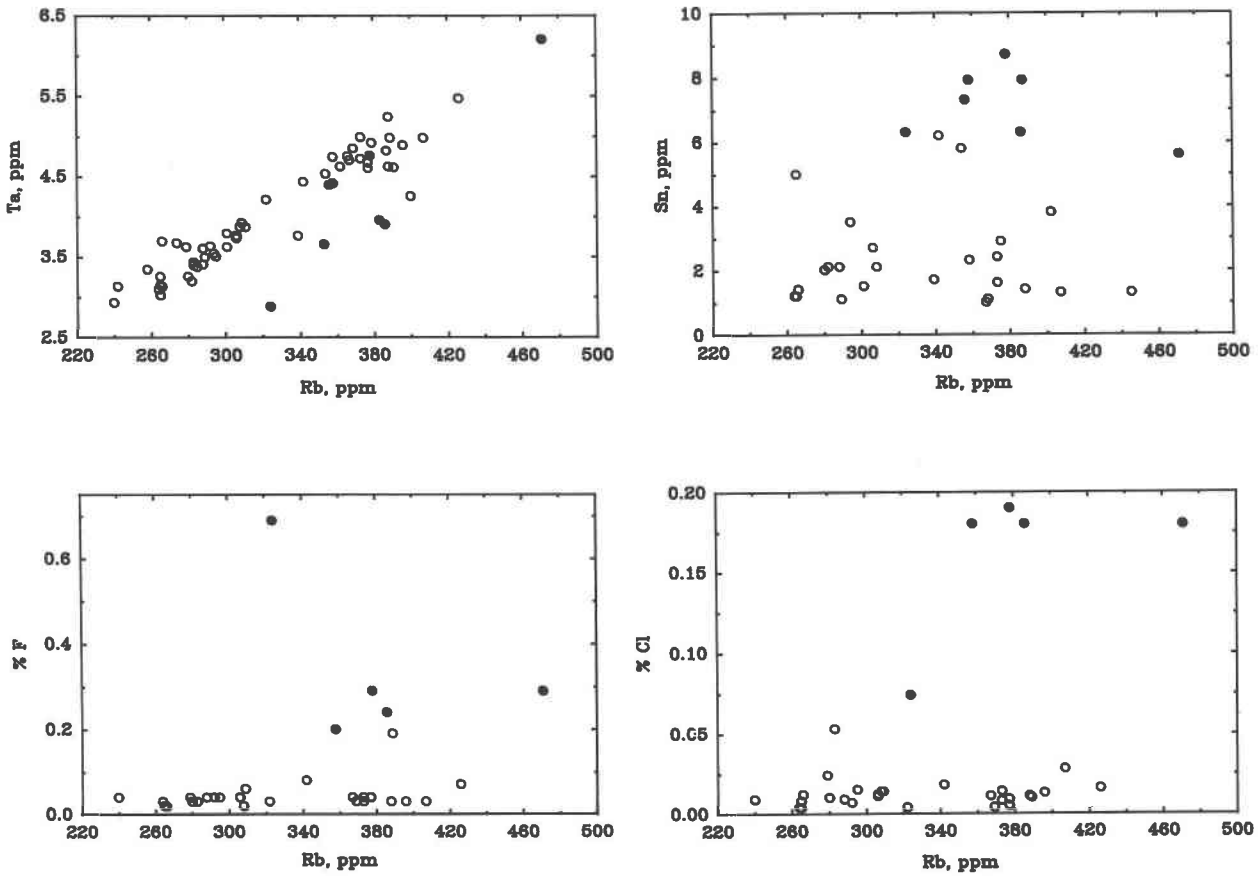

Fig. 3. Trace element variation diagrams for Ta, Sn, F, and Cl vs. Rb in whole rock felsites and vitrophyres of all mapped flows (Duffield et al., 1987) of the Taylor Creek Rhyolite. Open circles represent felsites; filled circles represent vitrophyres.

One might anticipate F-rich magma as a progenitor to nonmagmatic, vapor-phase topaz. Christiansen et al. (1986) report 0.38 wt% F in whole rocks from Taylor Creek Rhyolite. Constraints on F abundances in the four lavas used in this study are poor; there are no F data for vitrophyres from three of the four lava samples used in this study. Vitrophyre samples from other eruptive units of Taylor Creek Rhyolite contain about 0.2–0.3 wt% F (Fig. 3).

The whole-rock trace-element composition of the Taylor Creek Rhyolite varies considerably (Duffield et al., 1987). Ta vs. Rb concentrations define a relatively linear array on orthogonal plots, whereas Sn, F, and Cl vs. Rb exhibit scatter (Fig. 3). High correlation coefficients between pairs of elements may result primarily from magmatic processes, whereas low degrees of correlation may reflect variable mobilization of some elements during devitrification. Concentrations of relatively mobile elements are systematically lower in felsite than in vitrophyre counterparts (Fig. 3).

Whole-rock initial Sr isotopes are consistent with petrogenesis of the Taylor Creek Rhyolite involving melting of granulitic lower crust, followed by fractional crystallization of this melt and subsequent minor contamination of magma by upper crustal material. Initial $^{87}Sr/^{86}Sr$ of about 0.7046 and a Sr content of 3 ppm were variably changed to extremes of about 0.7131 and 20 ppm, respectively, by a relatively Sr-rich and radiogenic assimilant (Duffield et al., 1988; Reece et al., 1990). The most Sr-radiogenic Taylor Creek Rhyolite samples are also highest in Sr and lowest in Rb, Th, Ta, and Nb. In order to study a broad part of the spectrum of trace-element and Sr-isotope compositions, for glass inclusion study we selected two samples toward the Rb-poor end [the map or eruptive units Cabin Tank (herein abbreviated CBT) and Indian Creek (IDC), Fig. 2], which contain crystal-poor inclusions, and two samples toward the Rb-rich end [map units Doagy Canyon (DGC) and Boiler Peak (BLP), Fig. 2], which contain crystal-rich inclusions. Whole-rock compositions of these units are shown in Table 2.

Sample preparation and analysis

Whole-rock samples were crushed and sieved, and the −80 to +100 mesh fraction (roughly 150–230 μm grains) was selected for quartz and feldspar concentration. All glass inclusions discussed in this study are located in quartz phenocrysts. The crushed material underwent appropriate density fractionation in diiodomethane, fol-

TABLE 2. Major- and trace-element compositions of whole-rock samples from map units BLP and DGC of the Taylor Creek Rhyolite (Fig. 2)

Constituent	BLP	DGC
Weight percent		
SiO_2	77.22	77.02
TiO_2	0.11	0.11
Al_2O_3	12.41	12.47
FeO	0.95	0.93
MnO	0.05	0.04
MgO	0.11	<0.1
CaO	0.19	0.22
Na_2O	3.74	3.90
K_2O	4.79	4.85
P_2O_5	<0.02	0.03
F	(0.25*)	0.29**
Cl	(0.18*)	0.19**
LOI	0.37	0.12
ppm†		
Li	53	49
Be	12	13
B	16	20
Rb	386	376
Sr	13	13
Y	81	71
Nb	44	50
Cs	9*	11**
Ce	84	80
U	11*	14**
Th	38	35
Mo	5*	5**
Sn	8*	8**
Total (wt%)	100.46	100.34

Note: Analyses by X-ray fluorescence, specific-ion electrode (F, Cl), inductively coupled plasma AES (Sn, Mo, Li, Be), and instrumental neutron activation (Th, U, Ce, Cs) (Duffield et al., 1978). Major-element analyses are on a LOI-free basis; totals include major, minor, and trace elements. FeO = total Fe as FeO.

* Approximate mean concentration in vitrophyric Taylor Creek Rhyolite units other than BLP (Duffield, unpublished data). There are no vitrophyres from units *IDC* or *CBT*; vitrophyres from DGC were not analyzed for F. Devitrified Taylor Creek Rhyolite is greatly depleted in these elements, presumably because of loss during devitrification.

** Concentration in single vitrophyre from unit DGC.

† Parts per million by weight.

lowed by an acetone rinse, and then fractionated further by magnetic fractionation. The resulting quartz concentrate was etched with HF for several minutes at room temperature to remove attached groundmass, and the purified material was then mounted with araldite epoxy on round glass slides 1 in. in diameter. These grain mounts were polished with diamond powder and polishing oil, cleaned in methanol, and stored in a desiccator until analyzed. The polished surfaces were coated with C immediately before electron-microprobe analysis and were cleaned and coated with Au immediately before ion-microprobe analysis.

Electron microprobe

Glass inclusions were analyzed for Si, Al, Na, K, Ca, Fe, F, Cl, Mn, Ti, ±Mg by electron microprobe. Most inclusions were analyzed only once, because of their small size relative to that of the microprobe beam. Most analyses were conducted with a wavelength-dispersive, Cameca Camebax electron microprobe (Table 3) operated at 15 keV and 10 na beam current and with a 5- to 10-μm rastered beam. Data were corrected for atomic number, absorption, and fluorescence effects. Some analyses (Table 3) were conducted with a wavelength-dispersive, automated ARL-SEMQ microprobe operated at 15 keV and 50 na beam current and with a defocused beam 5–20 μm diameter. Data were collected and manipulated as suggested by McGee (1983). Beam size was adjusted with both microprobes to stay well within inclusions to avoid analyzing host quartz grains.

A hydrous, homogeneous glass prepared from distilled H_2O and natural topaz-rhyolite that was fused in sealed Au capsules was analyzed during each microprobe session to track possible inter- and intrainstrument variations. The relative 1σ precision of replicate analyses conducted on this glass with the Camebax and ARL microprobes is reported in Table 4. Comparison of the averaged concentrations shows that differences between all elements except for Na are within $\pm 1\sigma$ of the mean; differences in Na concentration between the two microprobes are within 2σ. Multiple analyses of this glass were conducted on a single spot to determine the extent of migration or "boil off" of Na, K, Cl, and F as a function of analytical time and beam size. Only Na exhibited detectable migration, amounting to <10% apparent Na migration when smaller beam sizes were used.

Ion microprobe

Glass inclusions were analyzed for H, Li, Be, B, Rb, Sr, Y, Nb, Mo, Sn, Cs, Ce, W, Th, and U by SIMS using a Cameca IMS 4f ion microprobe. The primary ion beam typically was somewhat wider than 25 μm, and we selected inclusions for analysis accordingly. We assume that this bias in inclusion size introduces no bias in typical inclusion trace-element compositions; major-element compositions are similar for inclusions that are <25–30 μm vs. those larger than this range. Analytical techniques are essentially the same as those described by Webster et al. (1987). Charging of the sample surface was accounted for during each analysis, and energy filtering was used to reduce mass interferences by the application of a positive 75 volt offset to the secondary ion signal. Analytical uncertainty for most elements, judged by precision associated with multiple analyses of glass standards, is about 15% of the reported concentrations (Table 5).

We assume that all H in inclusions occurs as OH^- and H_2O. H_2O standards, which consist of hydrous glasses of albite, orthoclase, and granitic compositions, were provided by Edward Stolper, California Institute of Technology. The total H contents (reported as H_2O) in these glasses were determined by infrared spectroscopy (Stolper, written communication), and we calibrated $H^+/^{30}Si^+$ measurements of the ion microprobe with respect to these contents to determine equivalent H_2O in the glass inclusions.

Standards for other elements measured by ion microprobe include natural obsidians, synthetic glasses (NBS nos. 610 and 612) prepared by the U.S. National Institute of Standards and Technology (formerly the National Bu-

reau of Standards), and several other synthetic glasses prepared by fusing topaz rhyolite and granitic rock powders with up to 4% distilled H_2O in sealed Pt capsules at 1000–1100 °C and 2–4 kbar. The trace-element contents of these powders are known from multiple analyses by wavelength dispersive X-ray fluorescence, energy dispersive X-ray fluorescence, atomic absorption, ion-selective electrode, and inductively coupled plasma AES and MS techniques.

The secondary ion yields for Na, Al, and K in the glass inclusions were determined periodically to verify that the analytical results for other elements were not influenced by matrix effects. Table 5 lists the range in ion yields for the complete set of standards and also reports the ion yields for an NBS glass standard. The reported uncertainties were determined from replicate analyses of a single standard glass. The atomic ion yield (IY) for a positively charged ion, Y, of mass X ($^{X}Y^{+}$) is calculated as

$$IY^{X}Y^{+} = \frac{(X)(\text{cts}^{X}\text{Y})(\%SiO_2)(\%\text{Si in } SiO_2)(\%^{28}\text{Si in Si})}{(28)(\text{cts}^{28}\text{Si})(\%Y_2O)(\%\text{Y in } Y_2O)(\%^{X}\text{Y in Y})}$$

where all values are in weight percent. Atomic ion yields for Na, Al, and K in anhydrous and hydrous granitic glasses typically range from 0.7 to 1.0, 1.9 to 2.4, and 0.7 to 1.1, respectively (Richard W. Hinton, personal communication, 1989). Because virtually all our data for Na, Al, and K fall within these ranges, we conclude that the secondary ion yields and our measured concentrations of H and other elements in the glass inclusions are not variably influenced by matrix effects and the concentrations are accurate.

Results

Sizes, frequency, and textures of inclusions

Glass inclusions in quartz phenocrysts range from 150 μm to somewhat less than 1 μm in diameter; inclusions 20–50 μm in diameter predominate. Modal counts of inclusions >1 μm in randomly selected grain mounts yielded about 360 inclusions in 1800 quartz grains for the sample from map unit BLP, 140 inclusions in 2500 grains from map unit DGC, 130 inclusions in 1100 grains from map unit CBT, and 260 inclusions in 1600 grains from map unit IDC. The modal counts were determined from one polished grain mount per sample. In the following discussion, the samples have been subdivided into those whose inclusions contain both glass and ≥40 vol% of microscopically visible daughter crystals (BLP and DGC) and those whose glass-rich inclusions contain no crystals (*CBT*) or a trace of crystals (*IDC*). For convenience, the abbreviated references to units whose inclusions contain all or nearly all glass are italic hereafter. The quartz grains studied include fragments of subhedral to euhedral phenocrysts.

Glass inclusions in feldspar phenocrysts are extremely rare, typically <15 μm in diameter, and usually are strongly devitrified (i.e., they contain minute quartz and potassium feldspar crystals). As a result, no analyses of glass inclusions in feldspar phenocrysts are given herein.

Inclusions from map units BLP and DGC. Two-dimensional shapes of inclusions in quartz phenocrysts from these two map units include irregular, round, square, and rectangular. Polyhedral shapes include both angular and rounded corners. The most common shapes are square and irregular with rounded corners. Nearly perfect negative crystals of quartz are also observed, but they are rare. Inclusions tend to occur as groups (as many as 15) in single grains from BLP and singly in grains from DGC.

Inclusions from both BLP and DGC contain clear glass and crystals. Nearly all inclusions in BLP quartz grains contain a small bubble-shaped void in addition to crystals; such voids are rare in DGC inclusions. We could not determine if the bubbles contain crystals on their walls, because of the high density of crystals in glass.

We visually estimate that inclusions in BLP typically contain <50% crystals by volume, whereas those in DGC contain noticeably more than 50%. Fluorite and F-rich biotite have been identified in inclusions of BLP. The biotite is pleochroic in shades of green, brown, and pink and typically is in contact with a coexisting bubble. Fluorite typically is in contact with the inclusion wall. If other crystalline phases are present in BLP, they have not been detected petrographically or with the SEM. F-rich muscovite is the only crystalline phase identified in inclusions of DGC.

Inclusions from map units *CBT* and *IDC*. Inclusion shapes in quartz phenocrysts from these two map units are the same as those from BLP and DGC. Virtually all inclusions from both *CBT* and *IDC* consist of clear glass and an associated bubble. Some of the inclusions occur along fractures, although most do not. We found no inclusions with daughter crystals from unit *CBT* during petrographic examination and backscattered electron SEM analysis at high magnification. Extremely fine-grained crystals are present in about half of the inclusions from unit *IDC*. These crystals are darker colored, always in contact with the bubble, and make up much less than 1 vol% of the inclusion. These crystals were never observed on the surface of polished inclusion mounts.

Bubble-shaped voids in glass occupy approximately 1–30 vol% of the studied inclusions; most bubbles represent approximately 5 vol% or less. We were unable to determine whether the bubbles contained vapor, but the bubbles do not contain visible crystals. Bubbles of similar size and occurrence associated with inclusions in phenocrysts from other rhyolites have been interpreted as resulting from differential shrinkage (Dunbar et al., 1989; Anderson et al., 1989). Furthermore, chemical evidence discussed below implies up to 15 wt% SiO_2 crystallized from the enclosed melt after trapping. We tentatively suggest that bubbles consisting of ≤5 vol% are a result of variable shrinkage during cooling and posttrapping quartz crystallization (discussed below). However, larger bubble volumes may indicate fluid saturation (± inclusion leakage) after trapping.

TABLE 3. Major, minor, and trace elements in glass inclusions in quartz phenocrysts from map units *IDC* and *CBT* of Taylor Creek Rhyolite

	Map unit *IDC* inclusion number							
	1	2	3	4	5	6	7	8
SiO_2	73.20	72.65	76.54	72.73	73.11	73.81	73.87	72.96
TiO_2	0.01	0.06	0.11	0.07	0.15	0.18	0.19	0.12
Al_2O_3	14.79	15.09	13.02	13.80	14.08	13.88	14.09	14.02
FeO*	0.62	0.10	0.16	0.26	0.31	0.35	0.14	0.13
MnO	0.04	0.03	0.02	0.07	0.05	0.03	0.06	0.03
MgO	—**	—	—	0.02	0.03	0.02	bdl†	0.01
CaO	0.16	0.49	0.40	0.41	0.46	0.40	0.30	0.46
Na_2O	3.54	4.03	3.43	3.97	3.93	3.90	4.21	3.97
K_2O	5.67	6.18	5.39	6.32	5.30	5.24	6.29	6.22
F	0.61	0.11	bdl	0.12	0.15	0.03	0.03	0.12
Cl	0.26	0.26	0.31	0.20	0.29	0.26	0.26	0.36
H_2O	1.10	0.40	0.55	1.90	1.00	0.90	0.60	1.60
Li	1600	750	740	920	780	480	310	560
Be	8.4	8.4	—	15	6.9	3.5	1.1	8.5
B	57	50	53	56	27	—	14	49
Rb	5	820	650	720	640	220	320	290
Sr	19	3.0	0.4	0.4	1.9	3.6	16	1.2
Y	200	150	100	110	69	28	23	120
Cs	19	33	22	18	18	6.9	3.8	12
Ce	370	100	47	52	54	30	40	64
Nb	7.7	69	52	63	64	25	18	11
Th	5.3	22	37	43	32	15	16	14
U	15	30	15	21	12	4.7	6.0	9.4
Mo	9.6	7.8	1.4	8.1	6.9	9.3	3.4	6.9
W	18	1.7	3.1	16	10	2.3	2.4	4.0
Sn	440	140	7.3	21	27	19	20	23
Totals	100.34	99.62	100.10	100.08	99.03	99.08	100.08	100.12

	Map unit *IDC* inclusion number							
9	10	11	12	13	14	15	16	17
74.73	72.81	72.92	73.57	73.05	72.89	73.88	73.18	72.47
0.09	0.10	0.12	0.13	0.06	0.18	0.13	0.15	0.11
13.31	14.22	14.65	14.05	14.36	14.21	14.27	14.73	14.74
0.07	0.46	0.18	0.28	0.49	0.37	0.16	0.29	0.17
0.08	0.05	0.12	0.08	0.06	0.09	0.07	0.01	0.02
bdl	0.01	0.02	bdl	0.01	0.02	0.02	0.02	0.02
0.52	0.50	0.52	0.44	0.50	0.48	0.47	0.52	0.48
3.74	3.87	3.76	3.97	3.99	4.00	3.92	3.15	4.22
5.93	6.45	6.25	6.48	6.20	6.33	5.68	6.37	6.25
0.34	0.18	bdl	0.04	bdl	0.15	0.05	0.28	0.22
0.33	0.34	0.36	0.34	0.34	0.26	0.33	0.34	0.29
0.85	1.00	1.10	0.60	—	—	—	—	—
650	110	1100	990	—	—	—	—	—
1.0	6.5	5.8	1.3	—	—	—	—	—
58	52	62	34	—	—	—	—	—
750	600	730	910	—	—	—	—	—
1.4	0.3	2.4	1.9	—	—	—	—	—
100	180	140	160	—	—	—	—	—
24	29	7.1	25	—	—	—	—	—
48	48	120	87	—	—	—	—	—
61	88	67	83	—	—	—	—	—
34	67	29	59	—	—	—	—	—
15	32	14	18	—	—	—	—	—
5.2	8.0	8.8	5.0	—	—	—	—	—
2.2	7.9	5.6	6.4	—	—	—	—	—
10	16	100	29	—	—	—	—	—
100.18	100.12	100.24	100.24	99.06	98.98	98.98	99.04	98.99

Note: SiO_2 through H_2O in weight percent, all other constituents in parts per million by weight. SiO_2 through Cl analyzed by electron microprobe, all others analyzed by SIMS. See text for discussion of analytical techniques. The totals include major-, minor-, and trace-element analyses. Inclusion numbers 1, 2, 3, 20, 21, 22, 27, and 28 were analyzed for major and minor elements with an ARL-SEMQ, and all other analyses were conducted with a Camebax electron microprobe. Sample locations in Figure 2.

* All Fe as FeO.

** Element not analyzed.

† Below detection limit.

‡ Inclusions 32 and 33 are located within the same quartz phenocryst; all other inclusions are located in separate quartz phenocrysts.

TABLE 3—*Continued*

	Map unit *CBT* inclusion number							
	20	21	22	23	24	25	26	27
SiO_2	74.16	72.77	74.26	72.79	73.62	73.54	73.49	73.62
TiO_2	0.14	0.11	0.13	0.11	0.11	0.10	0.15	0.09
Al_2O_3	13.95	13.97	13.90	13.72	13.72	13.34	14.45	14.08
FeO*	1.22	0.96	1.04	0.91	0.80	0.96	0.76	0.76
MnO	0.06	0.06	0.10	0.09	0.14	0.09	0.15	0.09
MgO	—	—	—	0.04	0.03	0.04	0.01	—
CaO	0.22	0.26	0.25	0.23	0.25	0.34	0.32	0.19
Na_2O	3.84	3.79	3.79	4.15	4.31	4.56	5.96	3.64
K_2O	5.34	5.52	5.48	5.80	5.83	5.55	5.96	5.87
F	0.06	0.03	0.17	0.10	0.24	0.14	0.23	0.19
Cl	0.22	0.28	0.23	0.30	0.30	0.30	0.34	0.31
H_2O	0.80	2.30	0.55	2.70	0.60	1.00	0.75	—
Li	320	180	890	740	610	620	690	—
Be	3.1	0.9	6.8	1.5	13	2.9	11	—
B	24	220	74	55	45	27	52	—
Rb	280	530	490	330	460	500	750	—
Sr	22	9.7	9.2	1.6	0.7	2.0	4.6	—
Y	5.2	19	90	43	84	110	57	—
Cs	10	20	7.9	18	19	15	26	—
Ce	41	38	61	44	77	54	36	—
Nb	80	4.1	31	49	53	54	93	—
Th	—	31	25	59	3.4	45	58	—
U	13	17	6.5	16	18	30	27	—
Mo	24	41	6.8	3.9	4.3	6.1	14	—
W	53	29	4.9	18	21	18	39	—
Sn	31	13	13	9.9	10	13	17	—
Totals	100.09	100.12	100.17	101.14	100.09	100.15	102.76	98.84

	Map unit *CBT* inclusion number									
28	29	30	31	32‡	33‡	34	35	36	37
73.71	72.81	72.42	75.56	72.58	73.61	73.20	73.08	72.98	72.93
0.11	0.12	0.15	0.09	0.09	0.15	0.12	0.14	0.06	0.13
14.14	13.91	13.92	13.15	13.92	14.49	13.83	14.00	13.90	13.72
1.19	1.00	0.89	0.84	0.82	0.76	0.80	0.68	0.70	0.91
0.11	0.11	0.13	0.14	0.08	0.08	0.10	0.03	0.10	0.09
—	0.04	0.02	0.01	0.02	0.01	0.02	0.02	0.01	0.04
0.24	0.27	0.31	0.31	0.24	0.32	0.23	0.24	0.23	0.23
3.82	4.44	3.36	3.84	4.12	3.48	4.01	3.93	4.06	4.19
5.63	5.69	6.00	5.58	5.78	5.96	6.05	6.17	6.18	5.94
0.19	0.23	0.16	0.15	0.15	0.23	0.06	0.15	0.27	0.18
0.32	0.26	0.26	0.32	0.34	0.34	0.29	0.27	0.30	0.30
—	—	—	—	—	—	—	—	—	—
—	—	—	—	—	—	—	—	—	—
—	—	—	—	—	—	—	—	—	—
—	—	—	—	—	—	—	—	—	—
—	—	—	—	—	—	—	—	—	—
—	—	—	—	—	—	—	—	—	—
—	—	—	—	—	—	—	—	—	—
—	—	—	—	—	—	—	—	—	—
—	—	—	—	—	—	—	—	—	—
—	—	—	—	—	—	—	—	—	—
—	—	—	—	—	—	—	—	—	—
—	—	—	—	—	—	—	—	—	—
—	—	—	—	—	—	—	—	—	—
—	—	—	—	—	—	—	—	—	—
99.46	98.88	97.62	99.99	98.14	99.43	98.71	98.71	98.79	98.66

Table 4. Electron microprobe comparison and associated analytical accuracy and precision

	ICP analysis*	ARL microprobe**	Analytical precision†	Camebax microprobe‡	Analytical precision†
SiO_2	69.3	68.89	0.4	69.08	0.4
Al_2O_3	13.1	13.61	2.2	13.29	1.5
TiO_2	0.04	0.02	45	0.04	33
FeO	0.88	0.87	1.3	0.81	2.5
MnO	0.04	0.07	66	0.06	22
MgO	0.00	n.d.§	n.d.§	0.05	13
CaO	0.38	0.36	2.1	0.34	3.3
Na_2O	4.3	4.09	2.7	4.42	1.3
K_2O	4.8	4.75	1.9	4.67	1.2
F	1.2	1.2	5.4	1.21	2.8
Cl	n.d.§	0.15	4.9	0.15	3.9
Total	94.0	94.09		94.12	

Note: Comparison of replicate analyses of the same chip of fused Spor Mountain, Utah, topaz rhyolite conducted at the U.S. Geological Survey, Reston, Virginia, with an ARL electron microprobe and at Edinburgh, Scotland, with a Camebax electron microprobe (as described in text). MgO, TiO_2, and MnO exhibit comparatively large imprecisions inasmuch as the concentrations of these elements are near detection limits. Total Fe as FeO.

* Analysis of natural rock powder (containing 1 wt% H_2O) by inductively coupled plasma spectrometry for all elements but Cl by Tony Irving; individual analyses and total have been adjusted assuming same material contains 6 wt% H_2O and a microprobe total of 94 wt%.

** Mean (in wt%) of 31 analyses conducted during seven analytical sessions.

† One sigma deviation (relative percent) about the mean.

‡ Mean (in wt%) of 38 analyses conducted during nine analytical sessions.

§ Constituent not determined.

Analytical results

Glass and coexisting crystals in inclusions of samples from units BLP and DGC were analyzed by electron microprobe as a form of geochemical reconnaissance of the crystal-bearing inclusions. Currently, we are conducting pressurized-heating experiments to rehomogenize inclusions to glass that may be representative of the composition of the original trapped melt. Biotite in inclusions from unit BLP contains up to 5.5 wt% F and nearly 0.7 wt% Cl (Table 6). The associated glass in inclusions is mildly peraluminous [molar $(Al_2O_3/Na_2O + K_2O + CaO) > 1$] and contains 1.6 wt% F. The glass in inclusions from unit DGC also is peraluminous, has an anomalous Na/K ratio, and contains 3.2 wt% F; associated muscovite contains 7.3 wt% F. The low silica contents (relative to glass-rich inclusions and host whole-rock compositions) of about 68–69 wt% in these glasses suggest considerable posttrapping crystallization of quartz has occurred, in addition to the posttrapping crystallization of the micas and fluorite, within inclusions. A combination of 60 wt% fluor-muscovite (which is the approximate modal amount as visually estimated) and 40 wt% of the associated glass for inclusions from map unit DGC would have a composition that is enriched in alkalis and considerably depleted in silica relative to the host whole rock. The analogous calculation for the fluorite- and biotite-bearing inclusions of unit BLP gives a similar result. We speculate that as lava temperatures decreased, posttrapping crystallization of quartz in these inclusions was substantial enough to saturate the remaining melt in fluorite, biotite, and muscovite. As discussed in following sections, some posttrapping crystallization of quartz apparently occurred in most Taylor Creek Rhyolite inclusions; however, the mass proportion of such crystallization in inclusions of *IDC* and *CBT* generally was far less than that deduced for units BLP and DGC. This may be partially the result of different cooling histories of the four eruptive units and partially the result of differences in F abundances. Glass inclusions containing enhanced F concentrations should experience more rapid diffusion of major elements through the trapped melt (Dingwell, 1984) and perhaps a greater degree of posttrapping crystallization.

Table 5. Ion yields and analytical precision for major and trace elements in SIMS standards

Element	NBS 610*	Ion yield range**	Analytical precision†
Na	0.78	0.7–1.2	2
K	n.d.‡	1.1–1.4	n.d.
Al	1.93	1.7–2.1	6
Li	1.00	0.6–1.2	7
Be	1.07	0.7–1.1	12
B	0.51	0.48–0.51	46
Rb	0.77	0.7–1.0	14
Sr	2.25	2.0–2.4	16
Y	2.70	2.0–2.7	20
Nb	1.00	0.8–1.5	14
Mo	0.64	0.64–0.66	20
Sn	0.15	0.1–0.3	13
Cs	0.46	0.3–0.7	15
Ce	1.77	1.4–1.8	8
W	0.35	0.29–0.35	20
Th	1.00	0.6–1.0	13
U	0.88	0.7–0.9	13

Note: Ion yields computed as described in text.

* National Bureau of Standards glass 610.

** Range in ion yields for all standards used.

† SIMS analytical error in percent relative (±1 sd of mean) as described in text.

‡ Element not determined.

Table 6. Compositions of glass and daughter minerals within glass inclusions

Constituent (wt%)	BLP glass*	BLP biotite	DGC glass**	DGC muscovite
SiO_2	68.95	37.01	67.73	42.96
TiO_2	0.12	1.70	0.04	1.23
Al_2O_3	15.57	16.36	18.03	31.07
FeO†	0.26	24.33	0.20	4.63
MnO	0.07	0.79	0.10	0.24
MgO	0.01	1.85	0.03	0.18
CaO	0.17	0.02	0.64	0.03
Na_2O	4.92	0.07	8.73	1.70
K_2O	6.00	9.03	0.38	8.74
F	1.62	5.50	3.22	7.26
Cl	0.34	0.69	0.58	0.03
Total	98.03	97.35	99.68	98.07

Note: Inclusions located in quartz phenocrysts from map units BLP and DGC of the Taylor Creek Rhyolite (Fig. 2). Analyses by Cameca Camebax electron microprobe; see text for analytical procedures. Analytical precision in Table 4.

* Average analysis for glass in four inclusions.

** Analysis for glass in one inclusion.

† All Fe reported as FeO.

TABLE 7. Mean compositions and standard deviations of whole rocks and of glass inclusions in quartz phenocrysts from samples of units *CBT* and *IDC*

	CBT		*IDC*	
Weight percent	(*n* = 18) Inclusion	(*n* = 2) Whole rock	(*n* = 17) Inclusion	(*n* = 1) Whole rock
SiO_2	73.30 ± 0.73	76.89 ± 0.63	73.52 ± 0.95	76.92
TiO_2	0.12 ± 0.02	0.14 ± 0.02	0.12 ± 0.05	0.15
Al_2O_3	13.89 ± 0.31	12.17 ± 0.36	14.19 ± 0.51	11.77
FeO*	0.89 ± 0.15	0.91 ± 0.03	0.27 ± 0.15	1.07
MnO	0.10 ± 0.03	0.06 ± 0.00	0.05 ± 0.03	0.03
MgO	0.02 ± 0.01	0.14 ± 0.00	0.01 ± 0.01	0.17
CaO	0.26 ± 0.04	0.30 ± 0.00	0.42 ± 0.11	0.30
Na_2O	4.07 ± 0.55	3.32 ± 0.23	3.86 ± 0.26	2.96
K_2O	5.80 ± 0.24	4.91 ± 0.03	6.15 ± 0.29	4.92
F	0.16 ± 0.07	(0.25**)	0.14 ± 0.15	(0.25**)
Cl	0.29 ± 0.03	(0.18**)	0.30 ± 0.05	(0.18**)
H_2O	1.10 ± 0.61	0.73 ± 0.54†	0.97 ± 0.42	1.28†
Total	100.00	100.00	100.00	100.00
ppm	(*n* = 7)	(*n* = 1, 6)	(*n* = 12)	(*n* = 1, 6)
Li	580 ± 230	49	750 ± 370	25
Be	5 ± 4	9	6 ± 4	9
B	71 ± 64	12	47 ± 14	23
Rb	480 ± 140	300 ± 33	600 ± 210	290 ± 24
Sr	7 ± 7	19 ± 3	4 ± 4	19 ± 3
Y	58 ± 35	69 ± 18	120 ± 53	71 ± 9
Nb	52 ± 27	47 ± 5	51 ± 27	46 ± 2
Cs	17 ± 6	9**	18 ± 6	9**
Ce	50 ± 14	100 ± 5	90 ± 90	91 ± 22
U	18 ± 8	11**	16 ± 8	11**
Th	42 ± 13	34 ± 4	31 ± 18	31 ± 2
Mo	14 ± 13	5**	7 ± 2	5**
W	26 ± 15	—‡	7 ± 5	—‡
Sn	15 ± 7	8**	71 ± 120	8**

Note: See Figure 2 for whole-rock sample locations. Analytical data for inclusions collected by electron microprobe and ion microprobe; see text for discussion. Analysis of whole rocks by X-ray fluorescence, specific-ion electrode (F and Cl), inductively coupled plasma AES (Sn, Mo, Li, Be), and instrumental neutron activation (Th, U, Cs, Ce). The *n* is the number of samples analyzed; concentrations include ±1σ. Totals do not include trace elements.

* All Fe as FeO.

** Approximate mean concentration in vitrophyric Taylor Creek Rhyolite units other than *IDC* or *CBT* (Duffield, unpublished data). There are no vitrophyres from units *IDC* or *CBT* for comparison. Devitrified Taylor Creek Rhyolite is strongly depleted in these elements, presumably by loss during devitrification.

† H_2O is assumed equal to loss-on-ignition at 900 °C.

‡ No data.

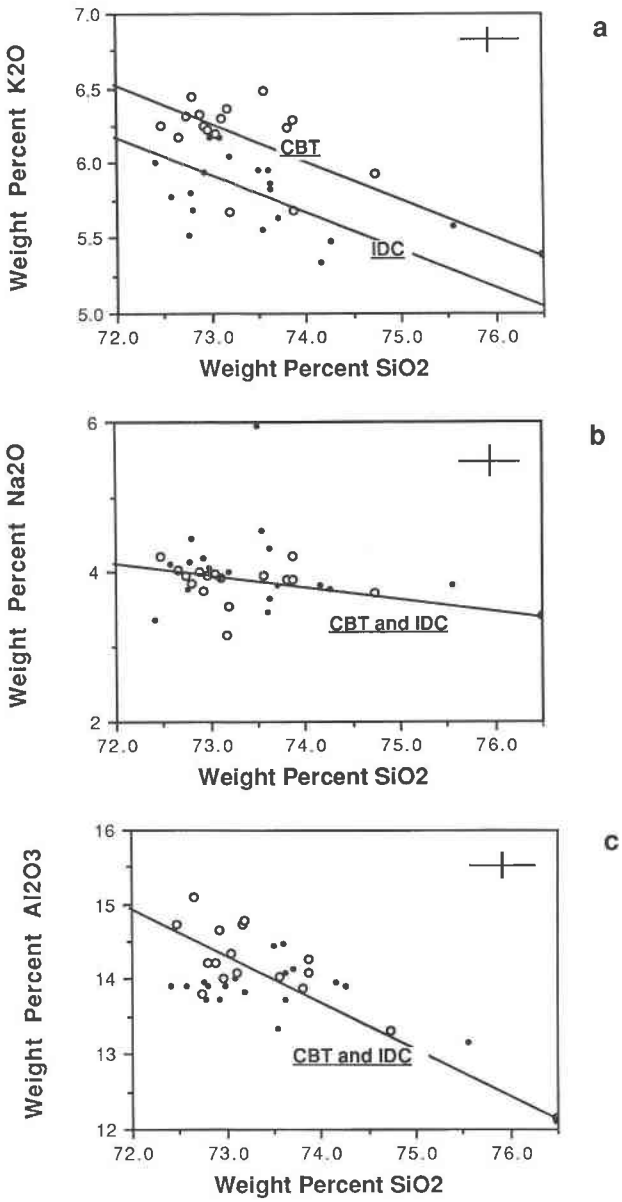

Fig. 4. Silica variation diagrams for K_2O (**a**), Na_2O (**b**), and Al_2O_3 (**c**) in glass inclusions of quartz phenocrysts from map units *CBT* (open circles; contains no crystals) and *IDC* (filled circles; contains <1 vol% crystals). The lines are interpretive and are based on the slope (Appendix 1) that expresses the predicted increase in K_2O, Na_2O, and Al_2O_3 and decrease in SiO_2 if quartz crystallized within inclusions after trapping. The lines are compatible with the general trend of the data and suggest that the observed variations in K_2O, Na_2O, and Al_2O_3 may result from posttrapping quartz crystallization (see text for discussion). The 1σ precision for analyses is shown in upper right corner of plot.

Seventeen inclusions from unit *IDC* and 18 from *CBT* were analyzed by electron microprobe. Twelve and seven of these, respectively, were also large enough for analysis by SIMS (Table 3). With the exception of the relatively minor constituents FeO and CaO, the concentrations of all major elements are essentially equal to their means in the two samples, within 1 sd (Table 7). Although all compositions are rhyolitic, silica is variably lower and Al_2O_3, Na_2O, and K_2O are variable and high in inclusion glass compared with the whole-rock composition of the host Taylor Creek Rhyolite (Table 7, Fig. 4). The trace crystalline phase in map unit *IDC* inclusions has not been analyzed because of its rarity and extremely small size. Inasmuch as these unidentified trace crystals are extremely fine grained, are not observed in all inclusions, and are undetectable on the surface of polished grain mounts, their presence in the inclusions will have little if any effect on major-element concentrations of these inclusions.

Mean concentrations of most trace elements in inclusions from units *IDC* and *CBT* are equal, within 1 sd of the means, to those of the corresponding whole rocks

(Table 7); however, many of these elements exhibit large ranges in concentration. Mean concentrations of Cs, Rb, Cl, possibly U, and especially Li are slightly to considerably higher in the glass of inclusions than in their whole-rock counterparts, although the fields for Rb, U, and Cs overlap somewhat. No vitrophyres from units *IDC* or *CBT* have been found during field examination. The vitrophyre analyses discussed below refer to eruptive units of Taylor Creek Rhyolite other than *IDC* or *CBT* (see notes of Table 7).

With one exception (Table 3, sample 1), concentrations of F in inclusions from units *CBT* and *IDC* are ≤ 0.34 wt%. The approximate mean concentration of F in vitrophyres from lavas other than *CBT* and *IDC* at Taylor Creek is 0.3 wt%. The difference in mean F contents between glass inclusions from flows *CBT* and *IDC* and vitrophyres from other eruptive units is negligible.

Discussion

A key question in studies of glass inclusions is whether the composition of the trapped glass is equivalent to that of its source melt. The chemical equivalence of melt and glass inclusion compositions and, hence, the utility of glass inclusion studies depends on whether the composition of the trapped melt has been modified from that of the bulk melt before or after trapping or both. For example, glass inclusions in quartz are unrepresentative of the bulk melt if the inclusions are located in quartz xenocrysts. However, trace-element concentrations in the glass inclusions of this study do not define multimodal populations, which might be expected if some of the quartz host grains were xenocrystic. We conclude, therefore, that our analyzed samples include no xenocrysts and the glass inclusions represent trapped Taylor Creek Rhyolite melt.

Processes that modify the composition of melt trapped in a quartz phenocryst include loss or gain of components through fractures in the host grain, loss of mobile constituents from the melt or glass to bubbles within inclusions, loss or gain of constituents by diffusion through the host grain, and partial crystallization of trapped melt, precipitating quartz or other minerals within an inclusion. As noted earlier, inclusions from DGC and BLP have been modified by considerable posttrapping growth of micas, fluorite, and quartz. Larhidi et al. (1980) report that melt inclusions located along cracks in phenocrysts from pantellerites and comendites lost Na $\pm$ K relative to other inclusions. As noted previously, some of the inclusions of our study occur along fractures, although most do not, and we observe no systematic compositional differences between these two modes of occurrence.

Beddoe-Stephens et al. (1983) suggested that brown-colored glass in inclusions may result from auto-oxidation of trapped glass that is facilitated by the diffusive loss of H if devitrification is not the cause. Inclusions from map units *IDC* and *CBT* contain colorless glass. Thus, the extent of H loss was insufficient to oxidize Fe strongly in glass (based on the criteria of Beddoe-Stephens et al., 1983).

Sommer (1977) and Beddoe-Stephens et al. (1983) noted that glass inclusions in quartz phenocrysts tend to be faceted and partly devitrified in slowly cooled deposits, whereas quickly cooled counterparts lack such features. Studies of inclusions in phenocrysts of other rocks (Takenouchi and Imai, 1975; Naumov et al., 1971; Clocchiatti and Massare, 1985) resulted in similar findings. Beddoe-Stephens et al. (1983) concluded that spheroidal glass inclusions in quartz phenocrysts indicate rapidly cooled materials with little or no posttrapping crystallization, whereas faceted inclusions and those with negative crystal forms indicate relatively slower cooling and more attendant posttrapping crystallization. As stated earlier, textural evidence in Taylor Creek Rhyolite inclusions suggests that quartz crystallized onto the walls of most inclusions after trapping. In addition, chemical evidence suggests that posttrapping quartz crystallization occurred within most inclusions.

Modified glass inclusion compositions

Silica-variation diagrams (Figs. 4 and 5) illustrate weak to strong negative correlations of silica with Al_2O_3, Na_2O, and K_2O for inclusions from map units *CBT* and *IDC* and less distinct negative correlations with H_2O, FeO, and CaO. These correlations are consistent with variable and partial posttrapping crystallization of melt as quartz. A quantitative measure of this effect can be calculated on the assumption that the original SiO_2 content of trapped melt was at least as high as the most SiO_2-rich inclusion in each map unit, 76.5 wt% and 75.6 wt% for samples from units *IDC* and *CBT*, respectively. The SiO_2 content of the whole-rock groundmass is calculated to be about 75 ± 0.5 wt% based on whole-rock composition, phenocryst compositions, and mode. If phenocrysts are removed in their modal proportions, the calculated SiO_2 content of the groundmass is increased somewhat. We have chosen 76.5 wt% to represent the silica concentration of the melt from which the phenocrysts grew, and given an initial SiO_2 content of 76.5 wt%, we can constrain changes in composition (Appendix 1).

The results of these computations express the predicted increase in the concentration of all melt constituents other than silica as quartz crystallizes from trapped melt and as the concentration of silica in melt decreases. Lines demonstrating the expected increase in concentrations of Al_2O_3, Na_2O, K_2O, CaO and FeO in trapped melt for inclusions from units *IDC* and *CBT* are shown graphically in Figures 4 and 5. The lines are interpretative and show that much of the variation in SiO_2, Al_2O_3, Na_2O, K_2O, and FeO in these inclusions may result from ≤ 15 wt% quartz crystallization after trapping. Furthermore, K_2O, CaO, and FeO contents of inclusions from *IDC* are different from those of *CBT*. The curves for CaO and H_2O are less successful in explaining their variations as the sole result of posttrapping quartz crystallization; other variables may have influenced their concentrations.

In addition, some of the negative correlation between

SiO_2 and other constituents of the glass inclusions could reflect chemical disequilibrium along the interface between growing quartz phenocrysts and adjacent melt. Loomis (1981), Delaney and Karsten (1981), and Green and Watson (1982) described the potential effects of chemical gradients along such an interface. Computations for the system anorthite-albite-H_2O demonstrate that substantial gradients may develop in granitic melts and cause the composition of trapped melt to differ from that of the melt located away from the margin of a growing crystal (Loomis, 1981). Bacon (1989) recently suggested that local disequilibrium may reduce solubilities of accessory phases within a differentiated, diffusion-dominated boundary layer along the margin of growing phenocrysts. If chemical gradients developed at the quartz-melt interface in Taylor Creek Rhyolite magma, one would expect such trapped melt to be relatively depleted in SiO_2, whereas other constituents would be relatively enriched, albeit to varying degrees, owing to differing diffusivities of each melt species. Because of their greater diffusivities, one might anticipate less enrichment in Na_2O and K_2O compared with Al_2O_3 (Bacon, 1989, his Fig. 4).

The near-exponential relationship observed between H_2O and SiO_2 (Fig. 5) may be explained in two ways. Glass inclusions from map units *CBT* and *IDC* that contain relatively high H_2O may have crystallized a correspondingly larger amount of quartz after trapping. Experimental studies demonstrate that rates of cation diffusion in silicate melts increase considerably with increase in dissolved H_2O (Watson, 1979). Thus, other variables being equal, high H_2O concentrations in inclusions may favor, kinetically, high degrees of posttrapping crystallization of quartz. An alternative interpretation is that inclusions that have undergone the most posttrapping crystallization of quartz may have also retained more of their original dissolved H_2O, perhaps because they were sealed to a greater extent by the daughter silica. Experimental and textural evidence discussed below suggests that inclusions from *IDC* and *CBT* may have lost some H_2O after trapping.

Calculated major-element compositions for glass-rich inclusions from units *IDC* and *CBT*, adjusted for $\leq 15\%$ posttrapping crystallization of quartz, are nearly the same as the compositions of their whole-rock hosts. This is compatible with experimental studies of F-rich, chemically-evolved, high-silica magmas (Clemens et al., 1986; Webster et al., 1987) that indicate quartz is the major silicate liquidus mineral in dry to H_2O-saturated melts at pressures ≤ 2 kbar. Furthermore, Manning (1981) demonstrated experimentally that the thermal stability of quartz increases significantly as the activity of F increases in H_2O-saturated haplogranite melts at 1 kbar. The experimental data indicate that at shallow crustal pressures quartz is the first mineral to crystallize from high-silica magmas that contain greater than 800–900 ppm F. The combined evidence suggests that quartz crystallization may have been the dominant process for producing variations in Al_2O_3, Na_2O, and K_2O in inclusions (Table 8).

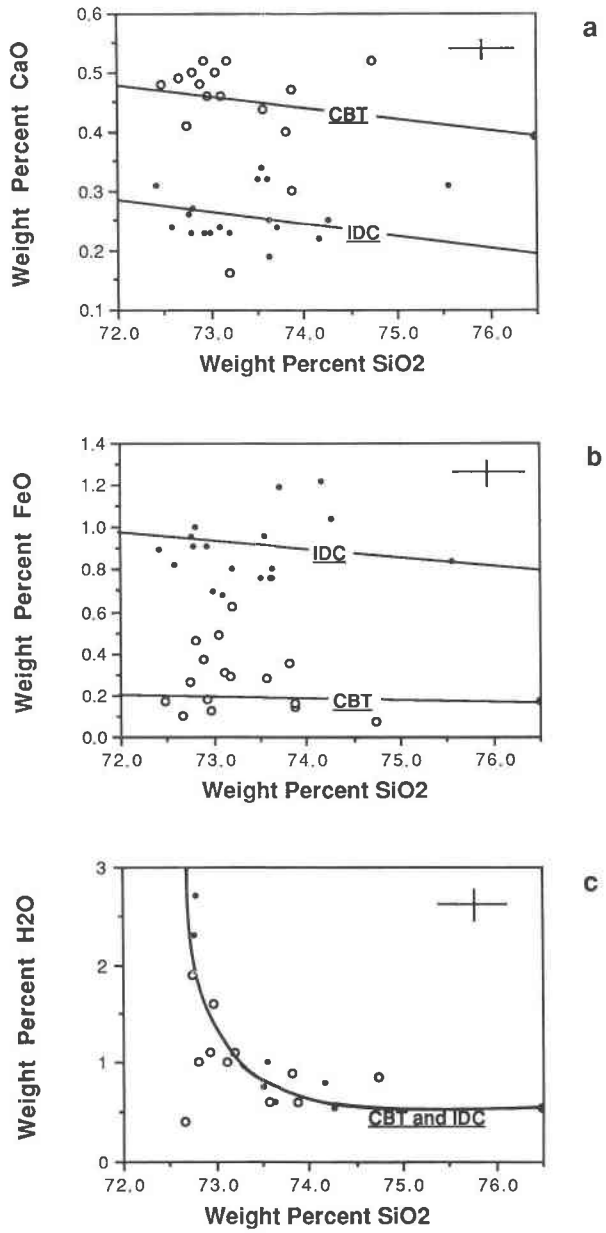

Fig. 5. Silica variation diagrams for CaO (**a**), FeO (**b**), and H_2O (**c**) in glass inclusions from map units *CBT* (open circles; contains no crystals) and *IDC* (filled circles; contains <1 vol% crystals). The lines in the figure were generated by the same method used in Figure 4, are compatible with the general trend of the data, and suggest that some of the observed variations in CaO and FeO may result from posttrapping quartz crystallization. The relationship between SiO_2 and H_2O is compatible with several interpretations (see text for discussion); the curve is interpretive. The 1σ precision for analyses is shown in upper right corner of plot.

No contacts are microscopically visible between the SiO_2 that may have precipitated on inclusion walls of the host quartz drains, presumably because of optical continuity and absence of foreign material at the contacts.

TABLE 8. Calculated major-element compositions of glass inclusions and compositions of whole-rock samples

Constituent	Inclusions		Whole rocks	
	CBT	*IDC*	*CBT*	*IDC*
Weight percent				
SiO_2	76.50	76.70	76.89 ± 0.63	76.92
TiO_2	0.11	0.11	0.14 ± 0.02	0.15
Al_2O_3	12.22	12.49	12.17 ± 0.36	11.77
FeO*	0.78	0.24	0.91 ± 0.03	1.07
MnO	0.09	0.04	0.06 ± 0.00	0.03
MgO	0.02	0.01	0.14 ± 0.00	0.17
CaO	0.23	0.37	0.30 ± 0.00	0.30
Na_2O	3.58	3.40	3.32 ± 0.23	2.96
K_2O	5.10	5.41	4.91 ± 0.03	4.92
F	0.14	0.12	(0.25**)	(0.25**)
Cl	0.26	0.26	(0.18**)	(0.18**)
H_2O	0.97	0.85	0.73 ± 0.54†	1.28†
Total	100.00	100.00	100.00	100.00

Note: See Appendix 1 for discussion of how glass inclusion compositions were adjusted for posttrapping quartz crystallization. Analytical data for inclusions collected by electron microprobe and ion microprobe, as explained in text. Analytical data for whole-rock samples by X-ray fluorescence and specific-ion electrode (F and Cl). See Table 4 for precision of electron microprobe analyses; whole rock precision is $\pm 1\sigma$. Inclusions are in quartz phenocrysts from samples of map units *CBT* and *IDC* adjusted for ≤15% posttrapping crystallization of quartz. Analyses of whole rocks are adjusted to totals of 100 wt% (Fig. 2).

* Total Fe as FeO.

** Approximate mean concentration in vitrophyric Taylor Creek Rhyolite units other than *IDC* or *CBT* (Duffield, unpublished data); there are no vitrophyres from units *IDC* or *CBT*. Devitrified samples are greatly depleted in these elements, presumably by loss during devitrification.

† H_2O is assumed to equal to loss-on-ignition at 900 °C.

Trace-element relations

Although the effect of posttrapping quartz crystallization on the major-element concentrations of glass inclusions can be substantial, the effect on trace elements is within analytical uncertainty. Many trace-element concentration ranges (Table 3) are far greater than analytical uncertainty.

The large variations in trace-element abundance may be attributable to a variety of causes. Traces of an unidentified mineral in some inclusions from unit *IDC* may have some effect on the observed range in trace element concentrations. Nonetheless, large variations exhibited by all-glass inclusions (from *CBT*) indicate that Taylor Creek Rhyolite melt was heterogeneous with respect to these constituents at the scale represented by the volume within which the quartz phenocryst grew. Furthermore, some of the variation is undoubtedly the result of changes in melt composition with increasing crystallization and fractionation; different glass inclusions may represent different times of trapping during the chemical evolution of the magma. Some of the variation may also be the result of contamination of melt by country rock, which is compatible with the observation of a broad range of initial whole-rock $^{87}Sr/^{86}Sr$ isotope ratios (Reece et al., 1990). The heterogeneity observed in glass inclusion compositions is clearly compatible with the minor yet ubiquitous dispersion from linearity on *X-Y* plots between such generally immobile elements as Ta, Th, and Nb in whole rocks (Fig. 3). Contrasts in FeO and CaO contents between the *IDC* and *CBT* inclusion populations may also be a result of these processes. In summary, we recognize the significance of the trace-element and minor-element variability in trapped melt, but at this time we cannot clearly define the cause or causes.

H_2O-undersaturated magma

Comparison of textures of Taylor Creek lavas with those of experimental products of like composition (Whitney, 1988; Cape Ann Granite) suggests that Taylor Creek magma was H_2O undersaturated during growth of quartz phenocrysts. Glass inclusions from glass-rich units *CBT* and *IDC* indicate that the melt, within which the quartz phenocrysts grew, contained ≤2.7 wt% H_2O; however, more than half of the inclusions contained <1 wt% H_2O. These low concentrations are not compatible with Whitney's (1988) experimental results. For example, at 2 kbar, 800 °C and with ≤1 wt% H_2O, the Cape Ann Granite contains ≥70 vol% crystals (Whitney, 1988), whereas Taylor Creek lavas at 800 °C contain roughly 10–40 vol% crystals. This suggests that, if the apparent pressure and temperatures of crystallization of Taylor Creek lavas are accurate, glass-rich inclusions from eruptive units *CBT* and *IDC* may have leaked some H_2 or H_2O after entrapment.

Furthermore, concentrations of $H_2O \leq 2.7$ wt% are low relative to predicted H_2O contents using the Burnham (1981) H_2O solubility model (described by Nekvasil, 1986). Predicted H_2O concentrations for H_2O-saturated Taylor Creek melt at 1.5 to 2 kbar range from 4.5 to greater than 5 wt%.

Additional evidence for the H_2O-undersaturated nature of magma erupted as these lava flows comes from a comparison of the Cl concentrations of glass inclusions of units *IDC* and *CBT* with experimental data for granitic systems, suggesting that the bulk melt had not equilibrated with a saline, aqueous fluid, i.e., the melt was not H_2O saturated, prior to trapping of inclusions. Experimental study has demonstrated that F-bearing, peraluminous granitic melts (Webster and Holloway, 1987, 1988) at 2 kbar and F-deficient, metaluminous granitic melts at 2–3 kbar (Malinin et al., 1989; Webster, 1991) contain ≤2600 ppm Cl (the chloride solubility limit) if the melt has equilibrated with a saline, aqueous fluid. F-deficient, metaluminous melts that have equilibrated with such fluids at ½ kbar do not contain greater than about 3100 ppm Cl (Malinin et al., 1989). Hence, natural metaluminous felsic melts at pressures of ½ to 3 kbar and containing greater than 3100 ppm Cl have not equilibrated with an aqueous fluid. We assume crystallization occurred at shallow crustal depths, i.e., at pressures ≤3 kbar, which is compatible with preliminary results of geobarometry based on compositions of F-rich amphiboles in Taylor Creek units. Nearly 40% of the inclusions contain greater than 3100 ppm Cl (Table 3); thus, the melt trapped in these inclusions had not equilibrated with an aqueous fluid prior to trapping. In summary, the Cl concentrations of inclusions from lava flows *IDC* and *CBT*

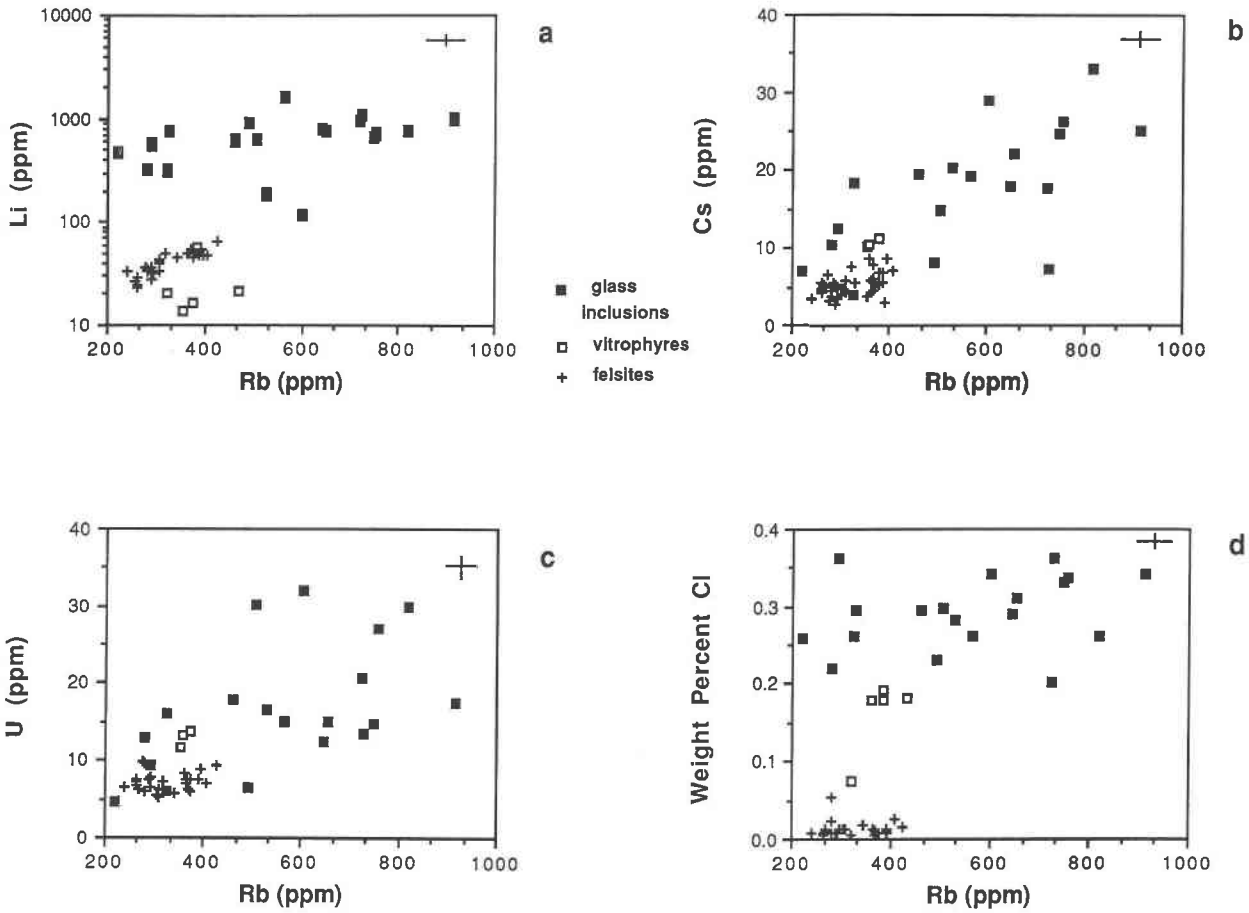

Fig. 6. Variations in Li (**a**) (log axis), Cs (**b**), U (**c**) and Cl (**d**) vs. Rb of glass inclusions in quartz phenocrysts (filled squares) for units *CBT*, containing no crystals, and *IDC*, containing <1 vol% crystals, for whole rock felsites (crosses) and for whole rock vitrophyres (open squares) of Taylor Creek Rhyolite. The felsite data include at least one analysis of each of the 20 holocrystalline lava flows; the vitrophyre data represent map units other than CBT or IDC. Li in inclusions is distinctly enriched above that in whole rock samples; most Cs abundances in inclusions are greater than that of whole rocks. Rb overlaps for each type of sample; however, mean Rb is highest in glass inclusions. Cl in glass inclusions is distinctly enriched above that in whole rock samples; most U abundances in inclusions are greater than that of whole rocks. The 1σ precision for analyses is shown in upper right corner of plot.

are consistent with other evidence suggesting that quartz phenocrysts grew and melt was entrapped in a H_2O-undersaturated magma.

Volatile saturation and exsolution may have occurred, however, as magma rose toward sites of eruption, after melt was trapped in quartz phenocrysts. Separation of a fluid phase from magma is consistent with the pyroclastic debris that is a ubiquitous early product of eruption of Taylor Creek Rhyolite magma. If the magma contained $\leq$2.7 wt% H_2O, as suggested previously, H_2O saturation would have occurred at $\leq$400 bars pressure, based on Burnham (1981).

Mobile constituents

Cl, Li, Rb, Cs, and possibly U are generally enriched in the inclusions relative to whole-rock samples from units *IDC* and *CBT* (Fig. 6). Li is uniformly 1–2 orders of magnitude more abundant in inclusions than in felsites or vitrophyres. Holland (1972) and Webster and Holloway (1988) showed that the distribution of alkali metals between a coexisting aqueous phase and granitic and F-enriched rhyolitic melts is strongly affected by the chloride concentration of the system. Thus, some Na, K, Li, Rb, and Cs may have exsolved from Taylor Creek Rhyolite melt as chloride complexes in an aqueous fluid phase after melt was trapped in phenocrysts. This loss of mobile melt constituents would have occurred at depths $\leq$1.6 km given the pressure constraints discussed above; this is different from the inferred depth of quartz phenocryst growth ($\approx$6 km).

If a fluid exsolved after melt was entrapped in quartz, the fluid was not enriched in F. F is enriched in a silicic melt relative to a coexisting aqueous phase if the melt contains <7 wt% F (Webster and Holloway, 1987), in contrast to the behavior of Cl. The relatively low concen-

trations of F in melt for flows *IDC* or *CBT* preclude strong enrichments in F for the exsolved aqueous fluid(s).

Comparison of concentrations of F, Cl, U, Cs, Mo, and Sn in glass-rich inclusions to those in whole rocks is complicated by the fact that these elements were mobilized and partly released from Taylor Creek Rhyolite during devitrification. Taylor Creek Rhyolite vitrophyres (from units other than *IDC* and *CBT*) are systematically richer in these elements than their devitrified counterparts (Figs. 3 and 6). From this relationship and in light of the glass inclusion compositions, we conclude that the magma from which phenocrysts of flows *IDC* and *CBT* grew contained at least 0.25 wt% F, 0.26 wt% Cl, 45 ppm B, 11 ppm U, 16 ppm Cs, 5 ppm Mo, and 15 ppm Sn. It is noteworthy, however, that inclusions from map units BLP and DGC contain F-rich minerals, sugeesting far greater halogen abundances were present in some fractions of Taylor Creek magma.

Relationships among halogens, Mo, Sn, and W

On a worldwide basis, hydrothermal ore deposits of Sn (± Mo and W) are associated with granitic rocks that are variably enriched in F ± Cl ± B (e.g., Kelly and Turneaure, 1970; Hesp and Rigby, 1972; Barsukov and Sushchevskaya, 1973; Ryabchikov et al., 1974). Sn mineralization within the Taylor Creek Rhyolite apparently is the result of mobilization and redeposition of Sn from exsolving vapors during the high-temperature devitrification of newly emplaced lava domes and flows (Burt and Sheridan, 1981; Lawrence, 1985; Eggleston, 1987; Duffield et al., 1990). The compositions of glass inclusions in quartz phenocrysts help constrain estimates of concentrations of ore metals in Taylor Creek Rhyolite magma.

Granites are considered to be the source of Sn for most magmatic-hydrothermal Sn deposits (Hutchison, 1983), although in some deposits both the pluton and the intruded host rocks may have supplied Sn to the ore fluids (Neiva, 1987). Granites typically contain an average of 3.5 ppm Sn (Wedepohl, 1969). Barren granites typically contain less Sn than fertile granites (e.g., Hutchison, 1983); for example, unmineralized granitic rocks associated with Sn deposits in Nigeria contain an average of 10 ppm Sn (Olade, 1980). Durasova (1967) distinguishes Sn-poor granitoids (mean of 3.3 ppm Sn) from Sn-rich granitoids (mean of 8.5 ppm Sn) genetically associated with Sn deposits. In addition, Sn deposits in Nigeria contain an average of 22 ppm Sn (Olade, 1980). Devitrified whole-rock samples of Taylor Creek Rhyolite contain about 1.5 ± 1 ppm Sn. The vitrophyre counterparts, however, contain about 8.5 ± 1 ppm Sn (Fig. 3), and the glass inclusions, with the exception of three samples with anomalously high Sn (Table 3, numbers 1, 2, and 11), contain about 15 ± 6 ppm Sn. This is greater than but similar to the Sn content of most Sn-rich granites. The three inclusions from unit *IDC* with >100 ppm Sn may reflect either high Sn concentrations in the unidentified phase or small-scale melt heterogeneity or both. We conclude that the Taylor Creek Rhyolite melt from which the quartz phenocrysts grew contained about 15 ppm Sn; however, it is unknown whether this Sn remained dispersed within the pluton inferred to underlie the Taylor Creek Rhyolite or was mobilized and concentrated.

Wedepohl (1969) reported that unmineralized granitic rocks worldwide contain 0.4–3.7 ppm W and 0.6–3.3 ppm Mo. Fourteen of the 19 glass inclusions in quartz phenocrysts of map units *IDC* and *CBT* have greater W concentrations than the maximum of this range, and eight of the 19 contain an order of magnitude more. Eighteen of the 19 inclusions also have greater Mo concentrations than the maximum for granitic rocks; three inclusions contain an order of magnitude more. Whole-rock samples of Taylor Creek Rhyolite vitrophyre contain about 5 ppm Mo. Taylor Creek Rhyolite melt apparently was somewhat enriched in W and Mo relative to unmineralized granitic rocks, and most of this material (no whole-rock data on W) was retained by the solidifying domes, flows, and resulting rocks during eruption and later cooling (though not during devitrification). In granitic systems, strong enrichments in Mo, W, and Sn may occur as disseminations within the granite (in oxides, sulfides, and other accessory phases) or be dispersed in hydrothermal fluids.

We have calculated correlation coefficients and applied factor analysis to the inclusion-composition data for map units *CBT* and *IDC*. Preliminary interpretations suggest that Mo exhibits a weak positive correlation with Sn; however, no other systematic relationships are apparent among Mo, Sn, W, H_2O, Cl, F, and B.

Conclusions

Glass-rich inclusions from Taylor Creek Rhyolite units *IDC* and *CBT* have major- and trace-element compositions broadly similar to those of host whole rocks; hence, the inclusions represent trapped melt. Major-element compositions of the inclusions have been variably modified to a small and systematic extent by ≤15 wt% posttrapping crystallization of quartz.

Inclusions in quartz from lava units BLP and DGC contain F-rich glass and substantial amounts of the daughter minerals fluorite, biotite, and muscovite. Quartz is inferred to be a daughter phase because of low concentrations of SiO_2 and negative correlations of SiO_2 with K_2O, Na_2O, and Al_2O_3. These inclusions are found only in lava flows that are near the highly evolved end of Taylor Creek Rhyolite lava compositions (high whole-rock Rb, Nb, Ta, and Th and low Sr and Ba). Semiquantitative reconstruction of inclusion compositions to their inferred initial compositions results in original compositions that are similar to whole-rock hosts except for extreme enrichments in F and Cl. The extreme halogen enrichments in inclusions of these two units implies strong differences in preeruptive abundances of F and Cl among the four lava flows studied.

Changes in trace-element concentrations in glass-rich inclusions resulting from ≤15 wt% posttrapping crystallization of quartz are about equal to the uncertainty as-

sociated with SIMS analysis. Concentrations of many trace elements in the glass-rich inclusions (from *IDC* and *CBT*) vary by factors of 2–10 or more. This may signify (1) variations in melt composition that accompany magmatic differentiation, (2) inhomogeneities in the melt on the scale of the magma volume within which the phenocrysts grew, and (3) assimilation of country rock which variably contaminated the magma.

H_2O contents of glass-rich inclusions are ≤ 2.7 wt%, and the highest H_2O concentrations may represent magmatic abundances during phenocryst growth. Comparison of experimental product textures (of Whitney, 1988) with those of Taylor Creek Rhyolite suggests that some H_2 or H_2O may have leaked from inclusions after trapping. Relatively high Cl concentrations in inclusions also suggest that phenocrysts grew in Taylor Creek Rhyolite magma under H_2O-undersaturated conditions.

Unlike other trace constituents, Rb, Cs, Cl, Li, and possibly U are enriched in glass-rich inclusions relative to whole-rock counterparts, and these constituents may have partially exsolved in an aqueous phase after phenocrysts crystallized and glass inclusions were trapped but prior to eruption. Alternatively, they were lost by late-stage degassing during eruption and cooling.

The compositions of glass inclusions that have not been significantly modified by posttrapping processes are most representative of natural melt. Measurement of H_2O in some glass inclusions may be the most accurate way to determine magmatic H_2O contents, and measurement of H_2O and Cl in inclusions is a powerful constraint on fluid saturation in silicic magmas. For rhyolites, mobile constituents as U, H_2O, F, Cl, Li, Rb, Mo, Sn, and Cs in vitrophyre should be viewed as minimum magmatic values. Glass inclusions in quartz phenocrysts are a large improvement over glassy volcanic rocks as representative samples of silicic melt.

Acknowledgments

Eric Christiansen and Jeffrey Rubin kindly provided rock powders of known compositions that we fused for use as ion-microprobe standards, and Ray Macdonald provided obsidians for trace-element standards. Sue Priest prepared the mineral concentrates. Jim McGee of the U.S. Geological Survey at Reston, Virginia, and Pete Hill and Stuart Kearns at Edinburgh directed the use of the electron microprobes. We appreciate useful discussions with Richard Hinton and John Craven at Edinburgh about ion-microprobe analysis of glasses. We greatly appreciate thoughtful and detailed reviews of the manuscript by Charles R. Bacon, Donald M. Burt, George E. Harlow, Edwin Roedder, Robert I. Tilling, Bruno Scaillet, and an unidentified reviewer for *American Mineralogist*. Any errors in the study are our own. Webster's contributions were supported by the U.S. Geological Survey Postdoctoral Research Associates program administered by the National Research Council in 1987 and by a grant from the North Atlantic Treaty Organization awarded in 1988.

References cited

Anderson, A.T. (1973) The before-eruption water content of some high-alumina magmas. Bulletin Volcanologic, 37, 530–552.

Anderson, A.T., Jr., Newman, S., Williams, S.N., Druitt, T.H., Skirius, C., and Stolper, E. (1989) H_2O, CO_2, Cl, and gas in plinian and ash-flow Bishop rhyolite. Geology, 17, 221–225.

Bacon, C.R. (1989) Crystallization of accessory phases in magmas by local saturation adjacent to phenocrysts. Geochimica et Cosmochimica Acta, 53, 1055–1066.

Barsukov, V.L., and Sushchevskaya, T.M. (1973) Evolution of composition of hydrothermal solutions in the formation of tin-ore deposits. Geochemistry International, 10, 363–375.

Beddoe-Stephens, B., Aspden, J.S., and Shepherd, T.J. (1983) Glass inclusions and melt compositions of the Toba Tuffs, Northern Sumatra. Contributions to Mineralogy and Petrology, 83, 278–287.

Burnham, C.W. (1981) Nature of multicomponent aluminosilicate melts. Chemistry and geochemistry of solutions at high temperatures and pressures, p. 197–229. Pergamon Press, New York.

Burt, D.M., and Sheridan, M.F. (1981) A model for the formation of uranium/lithophile element deposits in fluorine-enriched volcanic rocks. American Association of Petroleum Geologists Studies in Geology, 13, 99–109.

Burt, D.M., Bikun, J.V., and Christiansen, E.H. (1982) Topaz rhyolites—Distribution, origin, and significance for exploration. Economic Geology, 77, 1818–1836.

Chaigneau, M., Massare, D., and Clocchiatti, R. (1980) Contribution a l'etude des inclusions vitreuses et des elements volatils contenus dans les phenocristaux de quartz de roches volcaniques acides. Bulletin Volcanologique, 43, 233–240.

Christiansen, E.H., Sheridan, M.F., and Burt, D.M. (1986) The geology and geochemistry of Cenozoic topaz rhyolites from the western United States. Geological Society of America Special Paper 205, 82 p.

Clemens, J.D., Holloway, J.R., and White, A.J.R. (1986) Origin of an A-type granite: Experimental constraints. American Mineralogist, 71, 317–324.

Clocchiatti, R., and Massare, D. (1985) Experimental crystal growth in glass inclusions: The possibilities and limits of the method. Contributions to Mineralogy and Petrology, 89, 193–204.

Correa, B.P. (1981) The Taylor Creek Rhyolite and associated tin deposits, southwestern New Mexico, 105 p. M.S. thesis, Arizona State University, Tempe, Arizona.

Delaney, J.R., and Karsten, J.L. (1981) Ion microprobe studies of water in silicate melts: Concentration-dependent water diffusion in obsidian. Earth and Planetary Science Letters, 52, 191–202.

Dingwell, D.B. (1984) Investigations of the role of fluorine in silicate melts: Implications for igneous petrogenesis, 149 p. Unpublished Ph.D. thesis, University of Alberta, Edmonton.

Duffield, W.A., and Dalrymple, G.B. (1990) The Taylor Creek Rhyolite of New Mexico: A rapidly emplaced field of lava domes and flows. Bulletin of Volcanology, 52, 475–487.

Duffield, W.A., and du Bray, E.A. (1990) Temperature, size and depth of the magma reservoir for the Taylor Creek Rhyolite, New Mexico. American Mineralogist, 75, 1059–1070.

Duffield, W.A., Richter, D.H., and Priest, S.S. (1987) Preliminary geologic map of the Taylor Creek Rhyolite, Catron and Sierra Counties, New Mexico. United States Geological Survey Open-file Report 87-515, 1:50,000.

Duffield, W.A., Ruiz, J., and Nealy, L.D. (1988) Trace-element and isotope variations within the Taylor Creek Rhyolite, southwestern New Mexico. Geological Society of America Abstracts with Programs, 20, A281.

Duffield, W.A., Reed, B.L., and Richter, D.H. (1990) The origin of rhyolite-hosted tin mineralization: Evidence for the Taylor Creek Rhyolite, New Mexico. Economic Geology, 85, 392–398.

Dunbar, N.W., Hervig, R.L, and Kyle, P.R. (1989) Determination of pre-eruptive H_2O, F, and Cl contents of silicic magmas using melt inclusions: Examples from Taupo volcanic center, New Zealand. Bulletin of Volcanology, 51, 177–184.

Durasova, N.A. (1967) Some problems of the geochemistry of tin. Geokhimiya, 7, 802–812.

Eggleston, T.L. (1987) The Taylor Creek district, New Mexico: Geology, petrology and tin deposits, 473 p. Unpublished Ph.D. thesis, New Mexico Institute of Mining and Technology, Socorro, New Mexico.

Elston, W.E. (1968) Terminology and distribution of ash flows of the Mogollon-Silver City-Lordsburg region, New Mexico. Arizona Geological Society Guidebook III to southern Arizona, p. 231–240. Arizona Geological Society, Tucson, Arizona.

——— (1976) Glossary of stratigraphic terms of the Mogollon-Datil vol-

canic province, New Mexico. New Mexico Geological Society Special Publication, 5, 131–151.

Fries, C., Jr., and Butler, A.P. (1943) Geologic map of the Black Range tin district, New Mexico. U.S. Geological Survey Open-file Map, 1: 62500.

Fuhrman, M.L., and Lindsley, D.H. (1988) Ternary feldspar modeling and thermometry. American Mineralogist, 73, 201–215.

Green, T.H., and Watson, E.B. (1982) Crystallization of apatite in natural magmas under high pressure, hydrous conditions, with particular reference to 'orogenic' rock series. Contributions to Mineralogy and Petrology, 79, 96–105.

Hervig, R.L., and Dunbar, N.W. (1989) Direct determinations of volatile gradients in the Bandelier Tuff through analyses of melt inclusions. IAVCEI General Assembly, New Mexico Bureau of Mines and Mineral Resources Bulletin, 131, 129.

Hervig, R.L., Dunbar, N.W., Westrich, H.R., and Kyle, P.R. (1989) Pre-eruptive water content of rhyolitic magmas as determined by ion microprobe analyses of melt inclusions in phenocrysts. Journal of Volcanological Research, 36, 293–302.

Hesp, W.R., and Rigby, D. (1972) The transport of tin in acid igneous rocks. Pacific Geology, 4, 135–152.

Holland, H.D. (1972) Granites, solutions, and base metal deposits. Economic Geology, 67, 281–301.

Huspeni, J.R., Kesler, S.E., Ruiz, J., Tuta, Z., Sutter, J.F., and Jones, L.M. (1984) Petrology and geochemistry of rhyolites associated with tin mineralization in northern Mexico. Economic Geology, 79, 87–105.

Hutchison, C.S. (1983) Economic deposits and their tectonic setting, 365 p. MacMillan Press Limited, London.

Johnson, M.C., and Rutherford, M.J. (1989) Experimentally determined conditions in the Fish Canyon Tuff, Colorado, magma chamber. Journal of Petrology, 30, 711–737.

Kelly, W.C., and Turneaure, R.S. (1970) Mineralogy, paragenesis and geothermometry of the tin and tungsten deposits of the Eastern Andes, Bolivia. Economic Geology, 65, 609–680.

Kovalenko, V.I., Hervig, R.L., and Sheridan, M.F. (1988) Ion-microprobe analyses of trace-elements in anorthoclase, hedenbergite, aenigmatite, quartz, apatite, and glass in pantellerite: Evidence for high water contents in pantellerite melt. American Mineralogist, 73, 1038–1045.

Larhidi, N.R., Clocchiatti, R., Havette, A., Metrich, M., and Weiss, J. (1980) Chemical and thermometric study of hyperalkaline lavas (pantellerites and commendites of St. Pietre Island (southern Sardinia, Italy) (abs.). 1980 International Mineralogical Association Meeting, 131–132.

Lawrence, V.A. (1985) A study of the Indian Peas tin-bearing rhyolite dome-flow complex, northern Black Range, New Mexico, 112 p. Unpublished M.S thesis, University of Colorado, Boulder, Colorado.

Loomis, T.P. (1981) An investigation of disequilibrium growth processes of plagioclase in the system anorthite-albite-water by methods of numerical simulation. Contributions to Mineralogy and Petrology, 76, 196–205.

Lufkin, J.L. (1976) Oxide minerals in miarolitic rhyolite, Black Range, New Mexico. American Mineralogist, 61, 425–430.

Malinin, S.D., Kravchuk, I.F., and Delbove, F. (1989) Chloride distribution between phases in hydrated and dry chloride-aluminosilicate melt systems as a function of phase composition. Geochemistry International, 26, 32–38.

Manning, D.A.C. (1981) The effect of fluorine on liquidus phase relationships in the system Qz-Ab-Or with excess water at 1 kbar. Contributions to Mineralogy and Petrology, 102, 1–17.

McGee, J.J. (1983) $ANBA—A rapid, combined data acquisition and correction program for the SEMQ electron microprobe. U.S. Geological Survey Open-File Report 83-817, 45 p.

Naumov, V.B., Kovalenko, V.I., Kuz'min, M.I., Vladykin, N.V., and Ivanov, G.F. (1971) Thermometric study of inclusions of melt in topaz from topaz-bearing quartz keratophyre (ongonite). Doklady of the Academy of Sciences of the U.S.S.R., Earth Science Section, 199, 104–106.

Neiva, A.M.R. (1987) Geochemistry of greisenized granites and metasomatic schist of tungsten-tin deposits in Portugal. In H.C. Helgeson, Ed., Chemical transport in metasomatic processes, p. 681–700. Reidel, Boston.

Nekvasil, H. (1986) A theoretical thermodynamic investigation of the system Ab-Or-An-Qz(H2O) and implications for melt speciation, 268 p. Ph.D. dissertation, The Pennsylvania State University, University Park, Pennsylvania.

Noble, D.C., Smith, V.C., and Peck, L.C. (1967) Loss of halogens from crystallized and glassy silicic volcanic rocks. Geochimica et Cosmochimica Acta, 31, 215–223.

Olade, M.A. (1980) Geochemical characteristics of tin-bearing and tin-barren granites, Northern Nigeria. Economic Geology, 75, 71–82.

Pan, Y.S. (1974) The genesis of the Mexican-type tin deposits in acidic volcanics, 286 p. Unpublished Ph.D. thesis, Columbia University, New York, New York.

Price, J.G. (1985) Ideal site mixing in solid solutions, with an application to two-feldspar geothermometry. American Mineralogist, 70, 696–701.

Reece, C., Ruiz, J., Duffield, W.A., and Patchett, P.J. (1990) Origin of Taylor Creek Rhyolite magma, Black Range, New Mexico, based on Nd-Sr isotope studies. Geological Society of America Special Paper 246, 263–273.

Roedder, E., and Weiblen, P.W. (1970) Lunar petrology of silicate melt inclusions, Apollo 11 rocks. Proceedings of Apollo11 Lunar Science Conference, Geochimica et Cosmochimia Acta, 1, 801–837.

Rosholt, J.N., Prijana, and Noble, D.C. (1971) Mobility of uranium and thorium in glassy and crystallized silicic volcanic rocks. Economic Geology, 66, 1061–1069.

Ryabchikov, I.D., Durasova, N.A., and Barsukov, V.L. (1974) The role of volatiles in the mobilization of tin from granitic magmas. In M. Stemprok, Ed., Metallization associated with acid magmatism, vol. 1, p. 287–288. Ustredni Ustav Geologicky, Prague.

Sommer, M.A. (1977) Volatiles H_2O, CO_2, and CO in silicate melt inclusions in quartz phenocrysts from the rhyolitic Bandelier air-fall and ash-flow tuff, New Mexico. Journal of Geology, 85, 423–432.

Takenouchi, S., and Imai, H. (1975) Glass and fluid inclusions in acidic igneous rocks from some mining areas in Japan. Economic Geology, 70, 750–769.

Watson, E.B. (1979) Diffusion of Cs ions in water-saturated granitic melt. Science, 205, 1259–1260.

Webster, J.D. (1989) Pre-eruptive H_2O, F, Cl, B, and lithophile element abundances of topaz rhyolite magma, Spor Mountain, Utah, U.S.A. European Union of Geosciences Abstracts with Programs, 1, 279.

——— (1991) Fluid-melt interactions involving Cl-rich granites: Experimental study from 2 to 8 kbar. Geochimica et Cosmochimica Acta, in press.

Webster, J.D., and Holloway, J.R. (1987) Partitioning of halogens between topaz rhyolite melt and aqueous and aqueous-carbonic fluids. Geological Society of America Abstracts with Programs, 19, 884.

——— (1988) Experimental constraints on the partitioning of Cl between topaz rhyolite melt and H_2O and H_2O + CO_2 fluids: New implications for granitic differentiation and ore deposition. Geochimica et Cosmochimica Acta, 52, 2091–2105.

Webster, J.D., Holloway, J.R., and Hervig, R.L. (1987) Phase equilibria of a Be, U and F-enriched vitrophyre from Spor Mountain, Utah. Geochimica et Cosmochimica Acta, 51, 389–402.

Wedepohl, K.H. (1969) Handbook of geochemistry, vol. 2, p. 50-B-1–50-M-1. Springer-Verlag, Berlin.

Whitney, J.A. (1988) The origin of granite: The role and source of water in the evolution of granitic magmas. Geological Society of America Bulletin, 12, 1886–1897.

Zielinski, R.A., Lipman, P.W., and Millard, H.T. (1977) Minor element abundances in obsidian, perlite, and felsite of calc-alkalic rhyolites. American Mineralogist, 62, 426–437.

Manuscript received April 3, 1990
Manuscript accepted May 20, 1991

Appendix 1.

The average concentrations of major elements (wt%) in the glass inclusions from *IDC* and *CBT* (Table 7) have been adjusted for posttrapping quartz crystallization (Table 8) assuming that the melt from which the phenocrysts grew apparently contained 76.5 wt% SiO_2 and using the relationship

$$\text{concentration of } X = \frac{(\text{mass of } X)(100)}{(\text{mass of melt remaining})}. \quad \text{(A1)}$$

To compute the adjusted concentration of a given constituent in the melt, we determine the extent of posttrapping quartz crystallization (for every 100 g of melt prior to the onset of posttrapping quartz crystallization). For example, the unadjusted mean silica concentration of glass inclusions from *CBT* is 73.3 wt% (Table 7), and the number of grams of quartz crystallized after entrapment, represented by X in the equation

$$73.3 \text{ wt\% } SiO_2 = \frac{(100)[(76.5 \text{ g of } SiO_2 \text{ initially}) - (X)]}{(100 \text{ g melt initially}) - (X)} \quad \text{(A2)}$$

is approximately 12. Thus, the extent of posttrapping quartz crystallization is 12%. The adjusted concentration of any melt constituent, Na_2O for example, is computed by first determining the initial mass of Na_2O (signified by Y) in the melt:

$$4.07 \text{ wt\% } Na_2O = \frac{Y(100)}{(100 \text{ g melt initially} - 12 \text{ g } SiO_2 \text{ crystallized})}. \quad \text{(A3)}$$

The value of Y is then used to determine the initial concentration of Na_2O in the melt, prior to the onset of posttrapping quartz crystallization:

$$\text{initial concentration of } Na_2O = \frac{Y(100)}{100 \text{ g of melt initially}}. \quad \text{(A4)}$$